Herriott Cell and Robert Cell-based Multipass Optical Delay Devices for Binary White Cell-based True-Time Delay Systems

by

Yu Shi

Submitted to the Department of Electrical and Computer Engineering at OSU
March 29, 2013
In Partial Fulfillment of the Requirements for Graduating with Honors in Engineering and with Honors Research Distinction

Abstract

A number of novel low-loss and compact optical time-delay devices have been devised on the basis of the Herriott cell and Robert cell. We propose that these systems can produce discrete and variable time delays up to hundreds of nanoseconds. Time delays of this magnitude can be applied to many optical applications, but in this thesis, the focus is on incorporating our devices into optical true-time delay systems used for phased array antennas. This document presents derivations of the Herriott cell and Robert cell properties, and using their special properties, we designed modifications and coupling of the Herriott cell and Robert cell so that they could be readily implemented as delay elements for existing optical true-time delay systems. Historically, programmable long optical delays have been difficult to achieve with low loss in a small space. Modified and coupled Herriott cells and Robert cells are appealing because they have few components, small size and weight, very low loss, and robust alignment. We illustrate how modified Herriott and Robert cells can be set up such that they can be compatibly combined with White cell-based true-time delay systems.

Faculty Advisor: Prof. Betty Lise Anderson
Title: Professor of Electrical Engineering and Computer Science

Acknowledgements

This thesis describes my research for the past year and a half advised by Prof. Betty Lise Anderson. Throughout my project, I have received a great amount of assistance and guidance, and thus, there are many people to thank.

I show my utmost sincere gratefulness to Professor Anderson for her unremitting dedication to mentorship and enthusiasm for our research topic. It was with her continuous inspirations and encouragements that I was able to find true interest in photonics and derive true joy in conducting undergraduate research. I also thank Professor Anderson for her valuable tips and advices that prepare me well as I start my graduate studies next academic year. My tuition at Ohio State is definitely worth it.

I would also like to thank the professors that I have had at OSU, all of whom have laid the foundation for me to even begin this research project. I give my appreciation to every one of my friends at OSU for their care and support. I have learned a great amount from each of them not just about academics, but also about life. A big shout out to my group partners, Kevin Sahlin and Anand Holtkamp, for helping with the last portion of this project.

Lastly, I would like to dedicate this work to my beloved parents, Xianwei Shi and Jiayan Zhang. In 2000, they left a stable life in China and brought me to the U.S., hoping to provide me with a culturally diverse experience and the best higher education. Their sacrifices, love, and care are indispensible to everything that I have been able to achieve in college.

Contents

List of Figures

List of Tables

Chapter 1

Introduction

1.1. Phased Array Antennas

A phased array antenna (PAA) system is a broadband emission/reception system composed of a two-dimensional array of small-element antennas that can be independently activated. If all of the antennas are activated at once, the PAA system will emit a concentrated beam perpendicular to the plane of antennas due to the same principle as diffraction grating. However, if each element were time delayed by specific amounts, then the PAA system can have interference patterns that propagate at different directions without having to change the orientation of the PAA system. Therefore, the PAA system can be used as a stationary antenna or radar system, thereby eliminating the mechanical energy loss and frictional wearing of traditional rotating radar systems. [1]

To control the emission and reception directions of the phased-array antennas, each antenna element must be phase-shifted or time-delayed by a precise amount. One example is shown in Figure 1.1 [1], using an optical true-time delay system. In transmit mode, the RF signal to be sent is modulated onto a laser beam, which is then split into identical copies. Each light beam is given a specific time delay as determined by the beamforming processor. In receive mode, the array of laser diodes can pick up the signal from a certain direction. The optical TTD systems can then time-delay each element's signal according to the direction of reception to help reconstruct the

original signal. For narrowband waves, phase-shifting suffices as it treats a phase shift of 4π as equivalent to 0 radians. For broadband systems, true-time delays (TTD) must be used, in which a time delay that amounts to 4π at one frequency might be 3.5π at another. True-time delays prevent beam squinting, where different frequencies travel in different directions. [1]

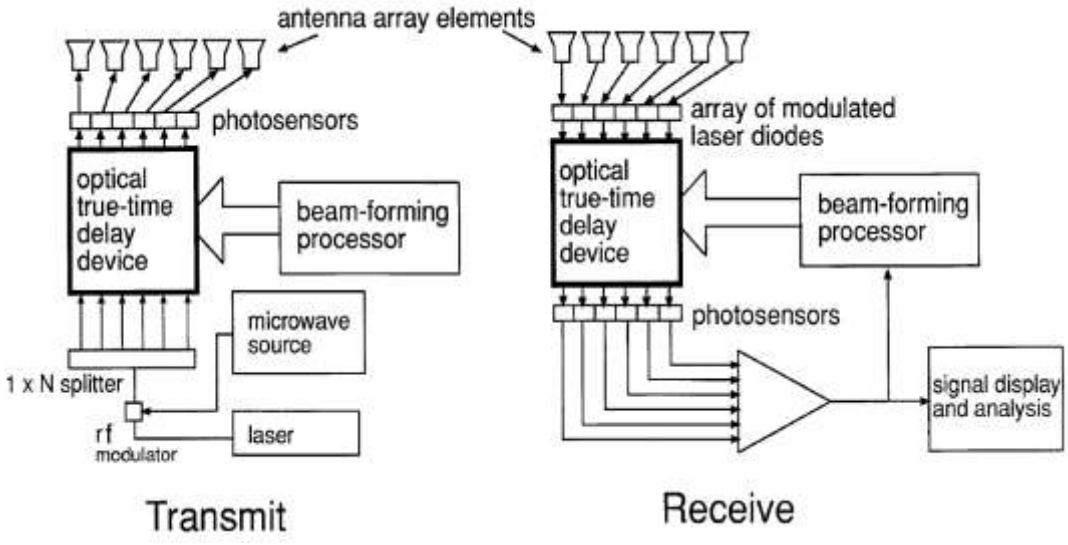

Figure 1.1: Combining a TTD system with transmitting and receiving PAA system [1]

In the past, TTD systems have commonly been implemented electronically. Before the desired electromagnetic signal gets propagated through the PAA, the signal is split into many smaller yet identical pieces. Each of the signal pieces then enters a TTD delay circuit shown in Figure 1.2. Depending on the state of each switch, the signal piece can experience a different time delay before it enters its corresponding antenna element. With an appropriate time delay applied to each of the signal pieces, all of the antenna elements in the PAA system can interfere in a way that produces a highly directional beam that sends the signal in the desired direction.

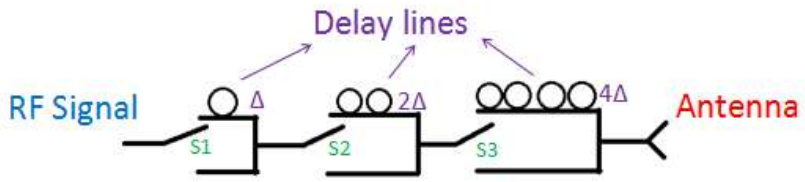

Figure 1.2: An example of a 3-bit delay circuit

Implementing long TTD electronically is unappealing because it requires long coaxial cables and wires and their associated weight and cost [1]. Nevertheless, a free-space approach to TTD using optical components based on the White cell was recently demonstrated, which has the lowest size, weight, and power of any known system. [2] In the next Chapter, we will describing the principles of operations of optical White cell-based TTD systems.

1.2. White cell-based TTD systems

1.2.1. Optical White cell

One of the optical TTD systems is one that implements optical White cells as its basis of design. Invented by John White in 1942, the White cell consists of three spherical mirrors A, B, and C with the same radii of curvature. [3] Shown in Figure 1.3, mirrors B and C are placed on the same side, and they are separated from mirror A by a distance equal to their radii of curvature. The center of curvatures (CC's) of mirrors B and C are also offset by a small distance. When a focused beams enters the White cell through the input turning mirror, it diverges alternatingly onto mirrors B and C, which refocuses the beam back onto mirror A, resulting in two non-

overlapping columns of spot patterns on mirror A shown as the solid dots in Figure 1.4 [4]. The White cell also accepts an array of focused beams, which forms two columns of spot arrays shown in Figure 1.4. In the next two sections, we will see that with the help of spatial light modulators (SLMs) or micro-electro-mechanical systems (MEMS), the structure of the White cell can be augmented to create true-time delay.

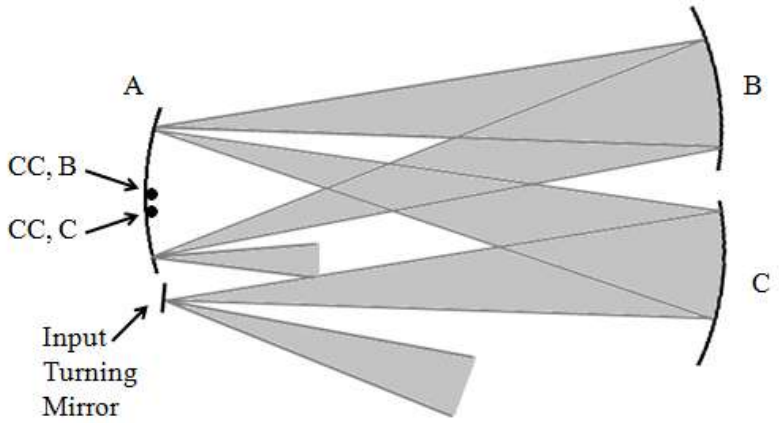

Figure 1.3: The structure of a White cell

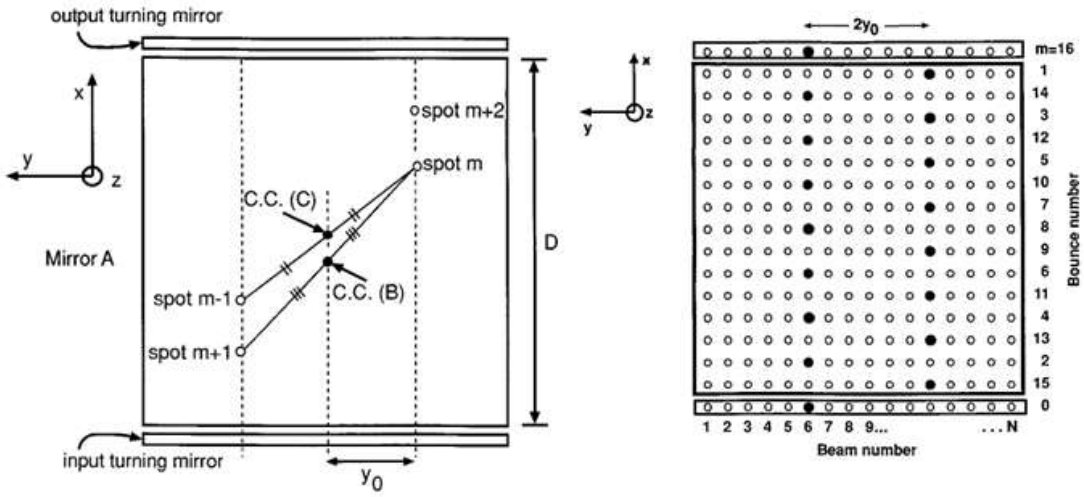

Figure 1.4: The spot pattern formed by a White cell [4]

1.2.2. Binary White cell using SLM

The structure of a simple special light modulator (SLM) White cell is shown below in Figure 1.5 [4]. Here, Mirror A of the White cell is replaced with a liquid crystal SLM and a lens whose focal length equals to that of the spherical mirrors B and C, preceded by a polarizing beam splitter. The polarization of the input beam array is chosen such that the beam passes through the beam splitter. Without changing the polarization of the beams, they are contained within the White cell. However, if, at any point of the operation, we would like to retrieve some beams before their full cycles of operation within the White cell are over, the specific pixels on the SLM can be activated to rotate the selected beams' polarizations by 90^{o}. These beams are subsequently reflected by the beam splitter as the outputs. The earlier a beam is reflected, the shorter of a time delay it has.

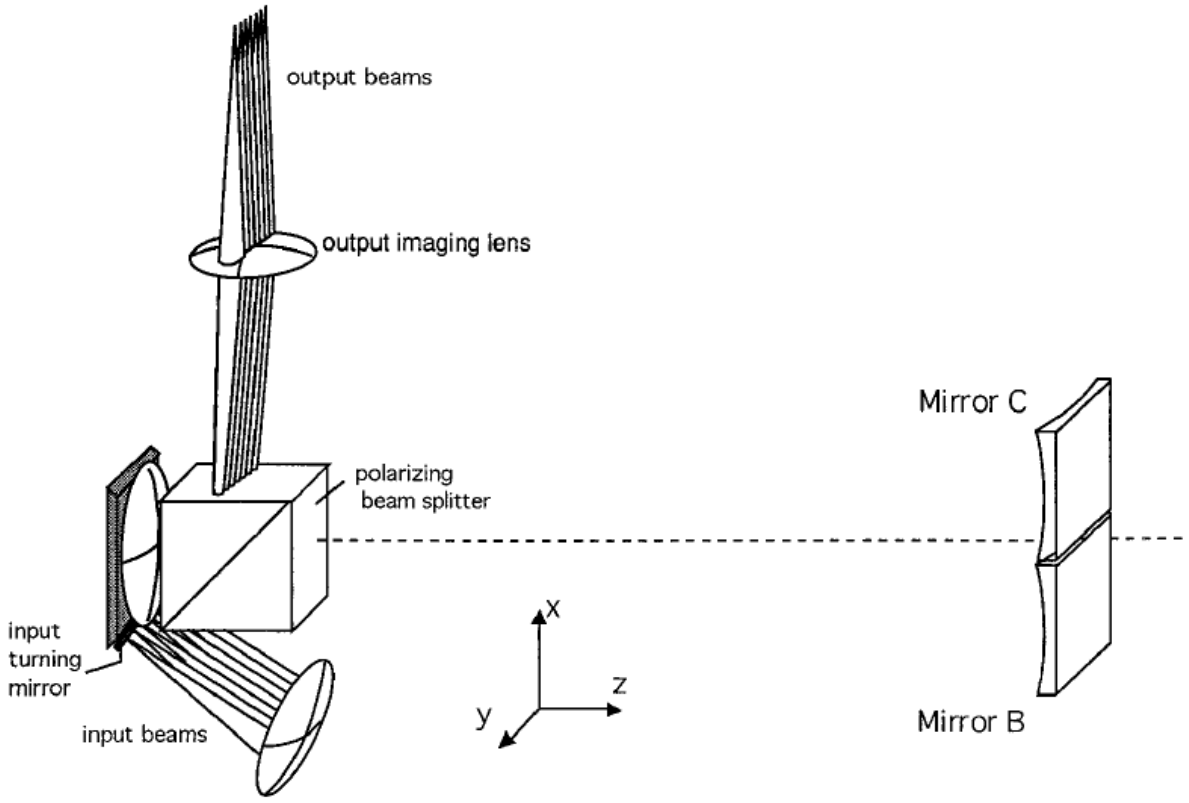

Figure 1.5: Structure of a simple White cell that implements an SLM [4]

The problem with the cell discussed above is that the output beams with different time delays would leave the cell from different locations and at different angles; thus it is difficult to collectively acquire that system's output beams. A better approach is to implement a binary White cell system using the SLM as the switching engine. When selected SLM pixels are activated, instead of sending the beams out of the system as outputs, we can create another set of White cell mirrors E and F that are identical to mirrors B and C. This new structure is depicted in Figure 1.6 [4]. When the beams are operating within the null cell with mirrors B and C, their reflections rely on the auxiliary mirror, which adds no extra time delay on the array of beams. After each cycle of operation, the beams will land onto the next row of the SLM pixels. However, during any cycle of operation, when selected beams from the beam array are switched into the

delay cell with mirrors E and F, their spot patterns would land on a delay plane conjugate to the auxiliary mirror. This delay plane can be the entrance to delay elements (glass blocks are shown). For the beams that are delayed, they are also returned back onto the next column of SLM pixels, which can then either keep the beams within the delay cell or switch them back into the null cell for the next cycle of operations.

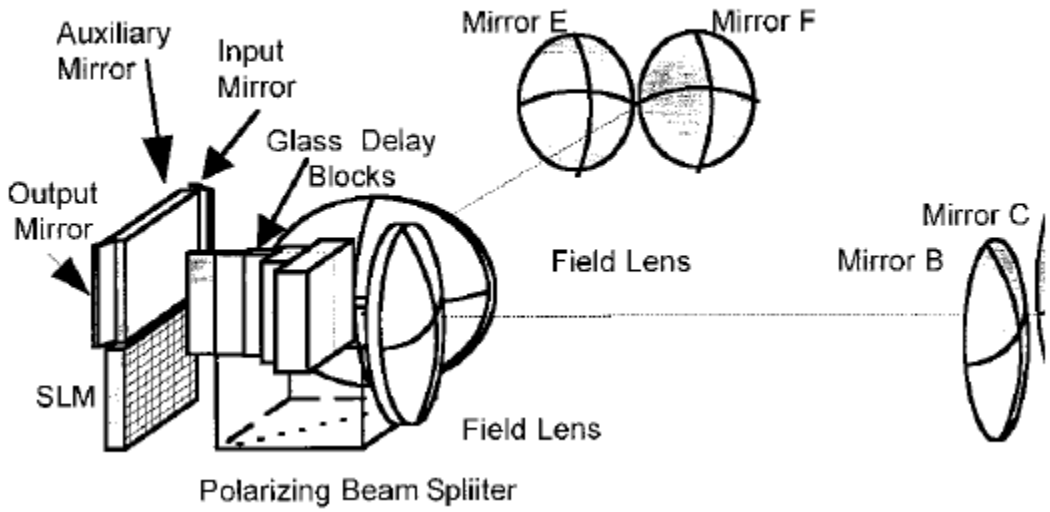

Figure 1.6: Binary White cell that uses an SLM [4]

In the case of Figure 1.6, the delay plane consists of glass blocks. These glass blocks have lengths that vary according to the White cell operation cycle, which allow the system to apply a different amount of optical time delay during each of its operation cycles. It should be mentioned that to maintain imaging conditions in the White cell, the delay blocks actually protrude slightly in front of the delay plane. [4] The time delays from each glass block is twice the amount from the previous block, so over N White-cell operations, the binary White cell system can produce 2^{N+1}-1 different time delays. [4]

1.2.3. Binary White cell using MEMS

A different way to implement a binary White cell-based TTD system is using MEMS mirrors as the switching element, which are arrays of micro mirrors that can be tilted electronically. The structure of this type of binary White cell is shown in Figure 1.7(a) [5], whose spot pattern is shown in Figure 1.7(b) [5]. The MEMS can serve as the switching engine between the null and delay cell, and the MEMS's switching mechanism is illustrated in Figure 1.7(c). When a row of focused beams enters the system via the input turning mirror, the beams diverge and hit Mirror B, which then refocuses these beams back on the first row of the MEMS. The MEMS pixels can then decide whether the beam operates within the null cell AB or the delay cell CD. If the MEMS remain untilted, the beam is reflected onto mirror A, which focuses the beam onto the auxiliary mirror, then back to mirror B, and finally onto the next row of the MEMS for its next cycle of operation. On the other hand, if the MEMS pixels are tilted, the selected beams would be sent onto Mirror C, which focuses those beams onto the inputs of the delay plane. The delayed outputs would reach mirror D, which also focuses the beams back onto the second row of the MEMS for their next cycle of operation.

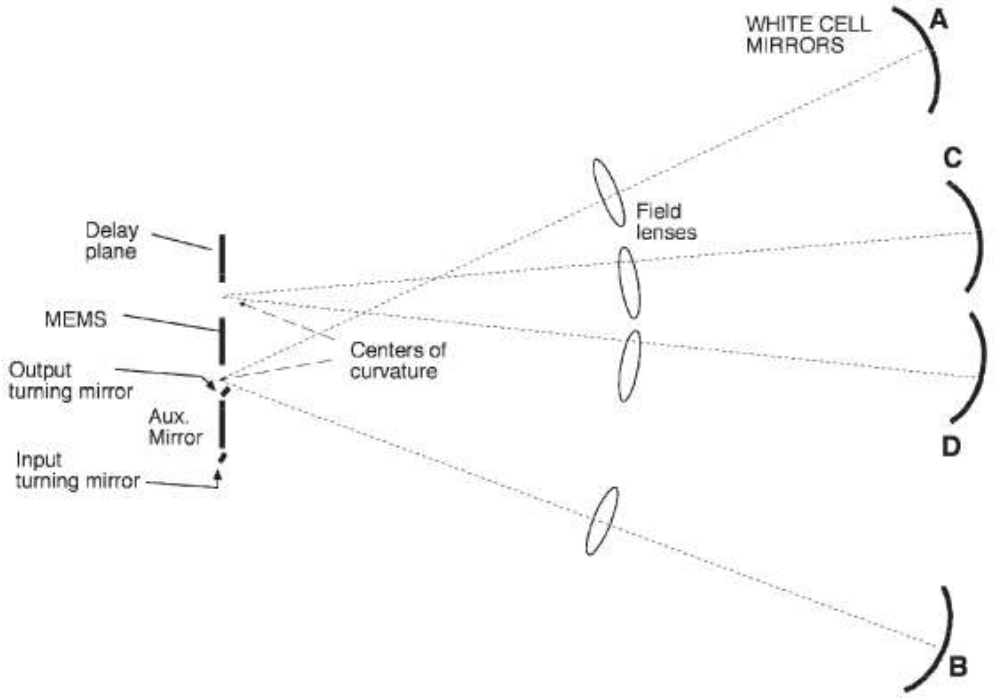
WHITE CELL MIRRORS
A
C
D
B
Field lenses
Delay plane
MEMS
Output turning mirror
Aux. Mirror
Input turning mirror
Centers of curvature

(a)

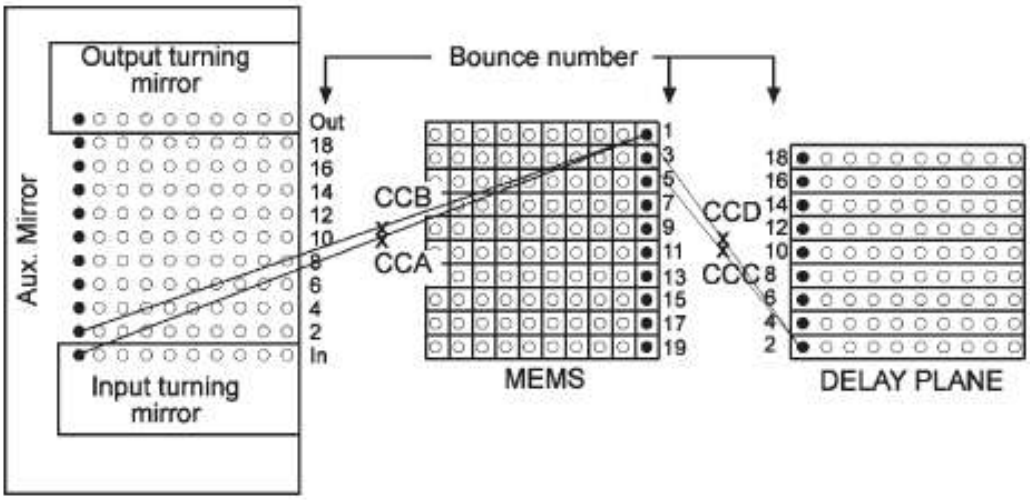
Output turning mirror
Input turning mirror
Aux. Mirror
Bounce number
Out
18
16
14
12
10
8
6
4
2
In
CCB
CCA
CCD
CCC
1
3
5
7
9
11
13
15
17
19
MEMS
DELAY PLANE

(b)

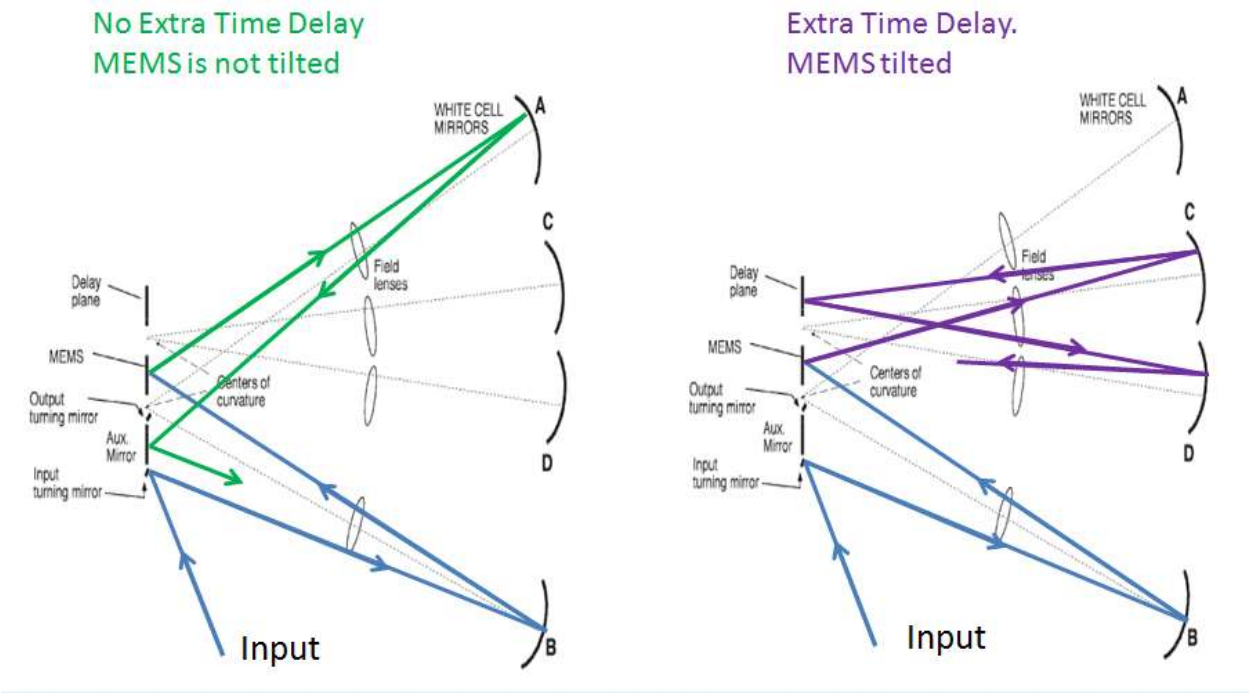

(c)

Figure 1.7: The binary White cell system (a) The structure and spot patterns of a binary White cell system. (b) The spot patterns created from a binary White cell. [5] (c) Illustration of how the MEMS control whether a beam is delayed or not

1.2.4. Delay Element Requirements and Existing Delay Devices

When adapting an optical delay device to the TTD system, we must make sure that the delay device has an input and output relationship that is similar to that of a mirror. This is to make sure that the input array spot pattern is not affected when beams travel into the delay cell. Ideally, the delay device should:

- Input and output the beam from the same location
- Preserve the slope of the beam while reversing its direction of propagation
- Focus the output beam if the input beam is focused.

With these guidelines, the following optical delay devices were implemented in existing optical TTD systems.

a) Dielectric blocks

Dielectric blocks of different lengths were used to produce different delays [6]. Because dielectric blocks have indices of refraction larger than that of air, they can slow the beam down to produce the desired delays. While short delays using these blocks are feasible, long delays are not easily achieved this way because the beam divergence requires very large blocks. Large blocks become heavy and expensive and are thus not practical.

b) Lens train

To achieve longer delays, a system consisting of a train of lenses has been used [6]. In one example of a lens train system, convex lenses with different focal lengths are placed in a line at increasing distances. When a focused beam enters the system, the lenses can reimage the spots onto planes called conjugate planes (CP). On each CP, a vertical mirror strip is positioned with respect to the bounce numbers. The distances between the CPs is proportional to 2^n, where n is the number of cycles in the White cell. While these lenses can achieve a long delay with relatively low loss, they consist of a large number of optical components that require very precise specifications. They are also difficult to align and occupy a large space.

c) Optical fibers

Another delay element that has been considered is optical fibers [6]. The way to obtain various delays is to set up fibers of different lengths proportional to the amount of delays, and rays are

guided into them to travel an appropriate length. Although rays do not experience a significant loss when they propagate within optical fibers, they will encounter a non-negligible attenuation when they enter and exit the fibers, and these losses accumulate as the various delay lines are switched in for a particular beam. Along with high losses for multiple entries into optical fibers, rays may also suffer from dispersion.

Thus, long, compact, and low-loss optical delays have been difficult to accomplish. Therefore, we aimed to design a system that reduces the shortcomings of delay elements. Inspired by Claude Robert's description of the Robert cell, we formulated our own mathematical way to derive the Robert cell's properties and invented various ways to modify the Robert cell to accomplish low-loss and long optical delay in a confined space.

1.3. Outline of the thesis

In the first part of the thesis, we will focus on the theoretical backgrounds of existing optical cells. We will begin with a comprehensive mathematical analysis of the Herriott cell, another multi-pass mirror system, and then we will apply the same method of analysis to the Robert cell. After summarizing the properties of the Herriott cell and the Robert cell, we present a series of modifications that can be applied to the Herriott cell and the Robert cell such that they can create long optical delays to be integrated into White-cell based TTD systems. A synopsis of each chapter is given below:

- In *Ch. 2 – Herriott Cell and Robert Cell*, we present a systematic and comprehensive analysis of both the Herriott cell and the Robert cell systems and derive their input and output ray properties. We start by studying the Herriott cell using the ray matrix and difference equation techniques, and we demonstrate the periodic property of the spot patterns formed within the Herriott cell. Next, we conduct an in-depth analysis on the Robert cell through the same mathematical techniques, and we derive the trajectory of the spot patterns within the Robert cell. We summarize the input and output relationships of a ray entering and exiting the Robert cell. We propose that the properties of the Herriott and Robert cells allow us to make adjustments to their structures so that they can be effectively used as delay elements in a TTD system.

- In *Ch. 3 – Modified Herriott cell and Robert cell devices*, we describe three modifications to the Herriott cell and Robert cell. For the Herriott cell, we propose to link two Herriott cell together through apertures as to achieve different time delays at different input locations. For the Robert cell, we modify the shape of the mirrors so that rays entering from different locations will experience different time delays. We then couple these adjusted Robert cells in two ways, the first of which allows the Robert cell to be combined with TTD devices, and the second of which can create ultra-long time delays up to potentially 100 ns.

- In *Ch. 4 – Summaries and Conclusions*, we summarize the results of our studies of the Herriott cell and Robert cell devices.

Chapter 2

Herriott Cell and Robert Cell

To study the properties of the Robert cell, we must first evaluate the principles of operations of its predecessor, the Herriott cell. In this chapter, we will first discuss the optical characteristics of the Herriott cell, and then we will derive the properties of the Robert cell.

2.1. Herriott Cell

A Herriott Cell [7] consists of two spherical mirrors (M1 and M2) on the same axis facing each other, as shown in Figure 2.1. An aperture is constructed on one of the mirrors at the location where the laser beam is introduced and extracted. The reflection patterns on both of the mirrors form ellipses, and the delay of the system is determined by the radii of the spherical mirrors and the distance between them.

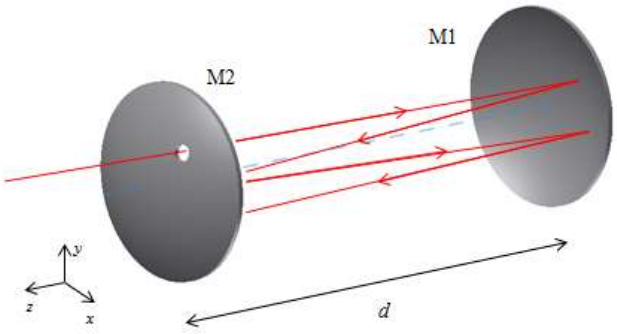

Figure 2.1: The structure of a Herriott Cell

There are a few interesting properties regarding to the reflection patterns contained inside a Herriott Cell. As described by Claude Robert and Donald Herriott, when the system intakes a laser beam that is nonparallel to the axis of the mirrors, the reflections result in an ellipse. With special input conditions, the pattern can be made circular. There is an equation describing the angles between two consecutive reflections, namely [8]:

$$cos\left(\frac{\varphi}{2}\right) = \sqrt{\left(1-\frac{d}{R1}\right)\left(1-\frac{d}{R2}\right)} \tag{2.1}$$

where Φ is the angle between two reflections (Figure 2.2), R_1 and R_2 are the radii of curvature for M1, M2 respectively, and d is the distance between the mirrors.

Noticeably, periodic reflection patterns can be obtained with special parameters within the Herriott cell. A graphical illustration of a periodic reflection pattern is shown in Figure 2.2, where the numbers show the number of reflections experienced by the beam. When the radii of the two mirrors are fixed, it can be seen that adjusting the distance d will produce a different Φ. Since Φ is the angle between two consecutive reflection spots, when $360/\Phi$ is equal to an integer K, then the system is periodic with the periodicity of K. That is, the locations of the spots on the

mirrors repeat themselves after *K* cycles after it bounces for a total 2**K* times on M1 and M2. In the case of a Herriott Cell, the beam reflects within the cell for *K* cycles and leaves the system from the location that it entered, which produces a total delay distance of 2**d***K*.

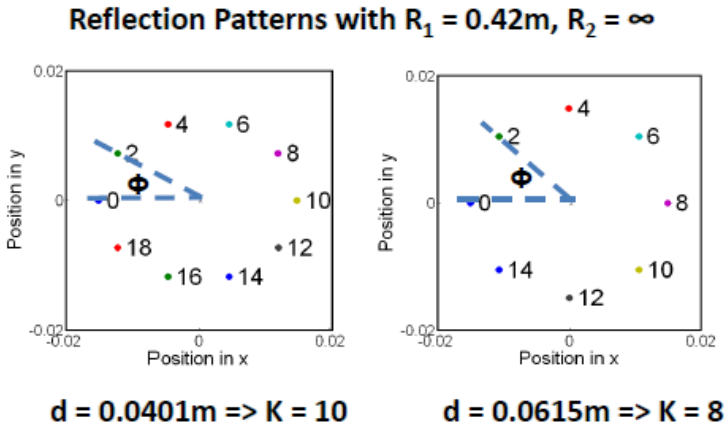

Figure 2.2: Two spot patterns formed with a Herriott cell at different mirror separations

2.1. 1. Ray Matrix Analysis

To find the position and the slope of the ray at any point in the system, we first employed the ray-matrix technique to analyze the Herriott cell system. [7] In a 3-dimensional system, a ray vector can be described by ***r*** shown in equation 2.2, where *x*, *y* are the positions in the *x* and *y* directions, and S_x, S_y are the slopes in the *x* and *y* directions, respectively.

$$\boldsymbol{r} = \begin{pmatrix} x \\ S_x \\ y \\ S_y \end{pmatrix} \tag{2.2}$$

In a Herriott Cell, when an input ray vector $\boldsymbol{r}$ goes through a cycle of reflections as shown in Figure 2.1, it first travels through a distance d onto M1, and then it is reflected by M1, and next it travels for another d, and finally it is reflected by M2. Thus, after one cycle, the new ray vector $\boldsymbol{r}_{n+1}$ can be described by Equation (2.3) [7]:

$$\boldsymbol{r}_{n+1} = T(R_2)*T(d)*T(R_1)*T(d)*\boldsymbol{r}_n = T*\boldsymbol{r}_n \tag{2.3}$$

where $T(R_2)$, $T(R_1)$ are the transfer matrices of *M2*, *M1* respectively; $T(d)$ is the transfer matrix of the ray traveling through a distance of d; $\boldsymbol{r}_n$ is the current state of the ray vector; $\boldsymbol{r}_{n+1}$ is the next state of the ray vector. Matrix T denotes the equivalent transfer matrix after a cycle of operation. $T(R)$ and $T(d)$ are 4 by 4 square matrices, and their matrix elements are shown below [7].

$$T(R) = \begin{pmatrix} 1 & 0 & 0 & 0 \\ -2/R & 1 & 0 & 0 \\ 0 & 0 & 1 & 0 \\ 0 & 0 & -2/R & 1 \end{pmatrix}, \quad T(d) = \begin{pmatrix} 1 & d & 0 & 0 \\ 0 & 1 & 0 & 0 \\ 0 & 0 & 1 & d \\ 0 & 0 & 0 & 1 \end{pmatrix} \tag{2.4}$$

2.1.2. Difference Equation Analysis

Another approach of analyzing the locations of the laser spots is to derive a mathematical model using coupled difference equations that describes the ray's positions and slopes. By observing the matrix elements shown in part (a), it can be noted that the ray vector elements $[x, S_x]$ are independent from $[y, S_y]$. Moreover, for spherical mirrors whose radii of curvatures are invariant under rotations about the z-axis (meaning they are not astigmatic mirrors), the total transfer matrix for the x and y directions are identical in the Herriott Cell. Therefore, the solutions in the x and y directions can be solved separately, and the form of the general solution for $[x_n, (S_x)_n]$ is

identical to [y_n, $(S_y)_n$]. The only difference in the final solution is the initial conditions [x_0, $(S_x)_0$] and [y_0, $(S_y)_0$].

When the matrix multiplications in Equation (2.3) are fully carried out, difference equations relating the position and slope in the *x*-direction are obtained and are given by:

$$x_{n+1} = A\, x_n + B\, (S_x)_n$$
$$(S_x)_{n+1} = C\, x_n + D\, (S_x)_n \tag{2.5}$$

with

$$A = 1 - \frac{2d}{R1}$$
$$B = 2d - \frac{2d^2}{R1}$$
$$C = \frac{-2}{R1} - \frac{2}{R2} + \frac{4d}{R1\,R2}$$
$$D = 1 - \frac{4d}{R2} - \frac{2d}{R1} + \frac{4d^2}{R1\,R2} \tag{2.6}$$

These equations can be solved by combining the equations into a single-variable second order difference equation as:

$$x_{m+2} - (A+D)*x_{m+1} + (AD - BC)*x_m = 0 \tag{2.7}$$

We then guess a homogeneous solution $x_n = x_0 * h^n$, where x_0 is the initial input location and h is a complex number. After solving for h, the final forms of the solution in position are simplified as:

$$x_n = x_0\, cos(\Phi * n) + k_2\, sin(\Phi * n)$$
$$y_n = y_0\, cos(\Phi * n) + l_2\, sin(\Phi * n)$$

with

$$k_2 = \frac{\left(1 - \frac{2d}{R_1} - b\right) x_0 + \left(2d - \frac{2d^2}{R_1}\right)(Sx)_0}{\sqrt{1 - b^2}}$$

$$l_2 = \frac{\left(1 - \frac{2d}{R_1} - b\right) y_0 + \left(2d - \frac{2d^2}{R_1}\right)(Sy)_0}{\sqrt{1 - b^2}}$$

$$\Phi = \arccos(b)$$

$$b = \frac{A + D}{2} \tag{2.8}$$

where A and D are the same as they were in Equation (2.6).

Via similar manipulations that produced equation (2.8), equation (2.5) also gives the progression of ray slopes of the Herriott cell as the following:

$$(S_x)_n = (S_x)_0 \cos(\Phi * n) + p_2 \sin(\Phi * n)$$

$$(S_y)_n = (S_y)_0 \cos(\Phi * n) + q_2 \sin(\Phi * n) \tag{2.9}$$

where p_2 and q_2 are constants related to the initial conditions of the beam.

2.1.3. Input and Output Relationships

The results from section 2.1.2 show that both the position and the slope of the ray patterns are periodic due to the presence of the sine and cosine terms. Therefore, under one full periodic cycle, the position and the slope of the ray return to their original value when the ray exits the Herriott cell from the same input aperture. In terms of ray matrices, this means that the Herriott cell has a ray transfer matrix equal to the identity matrix, which corresponds to the transfer

matrix of a mirror. This property is an indication that the Herriott cell can be chosen as a candidate delay device for an optical TTD system.

2.1. Robert Cell

As described by Claude Robert, the Robert cell system is a modified Herriott cell that produces a much longer time delay; thus, the Robert cell is a more preferable choice as a time delay element for a TTD system.

The structure of the Robert cell is shown in Figure 2.3 [9]. The difference between the Herriott Cell and the Robert Cell is that within a Robert Cell, mirror *M2* is split horizontally into two equal pieces: M2+, which is fixed, and M2-, which can be rotated about the vertical axis. The mathematical formulism for the Robert cell system is largely similar to that of the Herriott cell, and the ray matrix and difference equation techniques can both be applied to investigate this more complicated system [8].

As the ray circulates the cell, it may or may not be deflected by an extra amount due to the rotation of *M2*-. If the ray hits the upper mirror *M2*+, it will behave the same as in the Herriott Cell, and its positions and slopes can be described with the same formalism discussed in Section 2.1; if the ray hits the lower mirror *M2*- (which is rotated by an angle θ about the *y*-axis with respect to *M2*+), its slope in *x* will be deflected by an extra 2*tan(θ) after each cycle, while its position in *x* remains the same as that of a Herriott Cell. Note that the rotation of *M2*- only affects the formula in the *x* direction of the ray vector, and the evolution of the ray vector in the *y*

direction will remain intact. With this additional rule, the behavior of a ray inside a Robert Cell can be investigated using the same three techniques as the Herriott Cell.

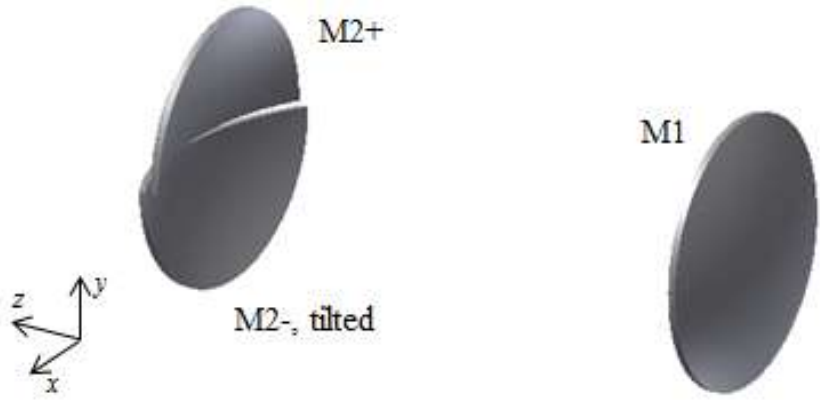

Figure 2.3: The structure of a Robert cell [9]

2.2.1. Ray Matrix Analysis

When a ray enters the Robert cell system, it bounces either between M1 and M2+ when $y > 0$ or between M1 and M2- when $y < 0$. When M2+ is struck, the cell acts as if it was a normal Herriott cell, and the same ray matrix shown in equation (2.4) can be applied. However, if the ray hits M2- tilted at an angle θ, the slope in the x direction will be further deflected by $2\tan(\theta)$. To account for this new term, the ray matrix for a spherical mirror in (1) is modified to be [9]:

$$T(R_2 -) = \begin{pmatrix} 1 & 0 & 0 & 0 \\ -2/R & 1 + \dfrac{2tan\,(\theta)}{Sx} & 0 & 0 \\ 0 & 0 & 1 & 0 \\ 0 & 0 & -2/R & 1 \end{pmatrix} \tag{2.10}$$

Now, the next state ray vector can be computed as [9]:

$$y>0: \quad \mathbf{r}_{n+1} = \mathbf{T}(R_2+)*\mathbf{T}(d)*\mathbf{T}(R_1)*\mathbf{T}(d)*\mathbf{r}_n = \mathbf{T}_+*\mathbf{r}_n$$

$$y<0: \quad \mathbf{r}_{n+1} = \mathbf{T}(R_2-)*\mathbf{T}(d)*\mathbf{T}(R_1)*\mathbf{T}(d)*\mathbf{r}_n = \mathbf{T}_-*\mathbf{r}_n \qquad (2.11)$$

Some examples of the Robert cell spot patterns are shown in Figure 2.4 [9], where the cell parameters are chosen such that they would produce patterns whose periodicity is 10 if they were used in the Herriott cell. These patterns show that as predicted, the *y*-positions of the spots are still periodic with a periodicity K=10. However, for every K cycles, when the *y*-position returns to its initial value, the spots' *x*-positions shift linearly by Δx, a quantity that decreases as θ decreases. The spots seem to swirl toward the center of the mirrors; upon reaching the center, they start to swirl out again. It is then appropriate to define every K cycles of the Robert cell to be one "swirl," and multiple swirls are denoted by N swirls.

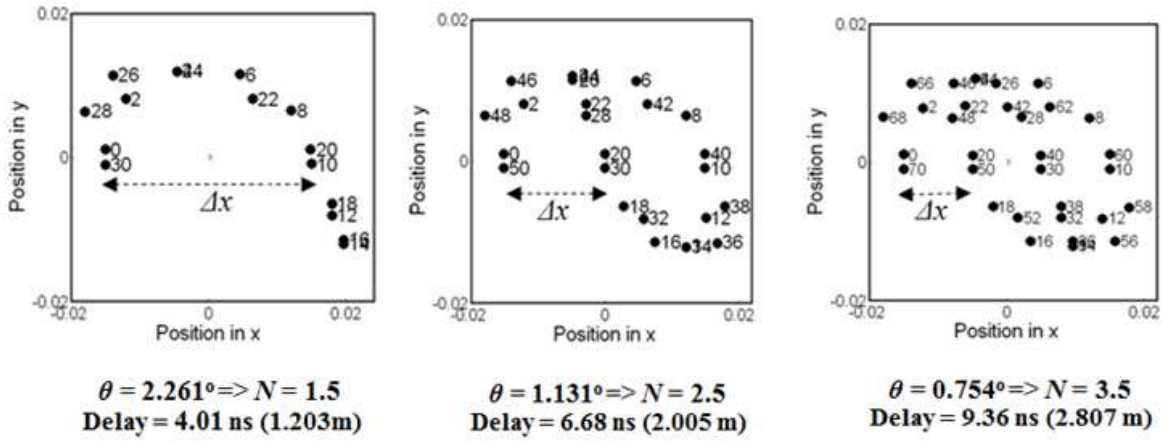

Figure 2.4: Spot patterns formed by the Robert cell under different angles of rotation. Cell parameters: R1 = 420 mm, R2 = ∞, d = 40.1 mm [9]

The results in Figure 2.4 also demonstrate that the Robert cell has the potential to be used as a compact delay element. For example, with the mirror separation of merely d = 40.1 mm, the beam traveled for 2.807 meters in the case where N = 3.5 and K = 10, which corresponds to a time delay of 9.36 ns. To achieve the same delay with the lens train requires the system to be 1.4 meters long and may require many lenses that have different focal lengths depending on the spot size and the number of spots. Thus, the Robert cell shows great promise in shrinking the physical dimensions of the true-time delay system.

On top of that, the amount of loss corresponding to the Robert cell is expected to be low because of the use of reflection. High-reflectivity coating on mirrors can be made better than anti-reflection coatings on lenses, and lenses have two surfaces instead of one. If the device is built with a dielectric mirror that has a reflectivity of 0.999, the amount of loss produced after 70 reflections in Fig. 6 (a time delay of 9.36ns) would merely be $1 - 0.999^{70} = 0.07 = -0.304$ dB.

2.2.2. Difference Equation Analysis

Recall that the lower mirror's angle rotation θ about the y-axis has no effect on the position or slope in the y direction. Therefore, equations (9) and (10) still hold for y and S_y.

The difference equation analysis in the x-direction, however, must be split up into two scenarios. When the ray hits M2+ and matrix $\mathbf{T}_+$ is applied to the ray vector, we can readily use equations (9) and (10). Nonetheless, if the ray hits M2- and $\mathbf{T}_-$ is applied, S_x will be further deflected by $2\tan(\theta)$, resulting in the following coupled difference equations [9]:

$$x_{n+1} = A\,x_n + B\,(S_x)_n$$

$$(S_x)_{n+1} = C\,x_n + D\,(S_x)_n + 2\tan(\theta) \tag{2.12}$$

where *A, B, C, D* inherit the same form as they did in (2.8).

When these equations are solved using the same procedures as we did in solving the Herriott cell, we obtain solutions that contain a homogeneous part comprised of sinusoidal functions and a particular part that varies linearly with respect to tan*(θ)*. The final forms of these equations are as follows [9]:

$$x_n = k_1 \cos(\Phi * n) + k_2 \sin(\Phi * n) + \frac{B}{1-b}\tan(\theta)$$

$$(Sx)_n = p_1 \cos(\Phi * n) + p_2 \sin(\Phi * n) + \frac{(1-A)}{(1-b)}\tan(\theta) \tag{2.13}$$

The values k_1, k_2, p_1, and p_2 are determined by the initial conditions [$x0$, Sx_0] and cell parameters, and *A, B, b, Φ* are all identical to their forms in (2.6) and (2.8).

2.2.3. Interpretation of the difference equation solutions

The interpretation of the Robert cell solutions is not a trivial task, because in different cycles, the ray may strike M2+ or M2-, each of which corresponds to a different solution. The result of this is the analysis of piece-wise discrete parametric equations in the *x* and *y* directions. To simplify our analysis, we choose to examine the case where *Φ* satisfies the periodicity condition, where $360/\Phi = K$ = the period. We further require *K* to be an even integer.

a) Solutions in the y-direction

In the *y*-direction, the position and slope are independent of the rotational angle θ, so the sinusoidal solutions in *y* shown in (2.8) and (2.9) can be used regardless of whether the ray hits M2+ or M2-. Thus, for every *K* cycles (or full *N* swirls), the position and slope in *y* returns to their input values; for an extra *K*/2 cycles (or at *N*+1/2 swirls), the sinusoidal nature of the solutions implies that the position and slope in *y* would simply be the negative of the input values.

b) Solutions in the x-direction

The solutions in the *x*-direction require a more systematic treatment. When the ray travels on M2+, we need to use (2.8) and (2.9), whereas a ray that lands on M2- would need solutions in (2.13). Because the solutions for both the position and slope take on the same form, we can start analyzing the behavior of the *x*-position and obtain the same insight for the *x*-slope.

Assume that a ray is sent into the system with $x = -x_o$, $y > 0$, and $Sy > 0$, so that it begins its operations on M2+. To further simplify our discussion, we choose a slope *Sx* such that it eliminates the sine term in equation (2.13). If we restrict our analysis to multiples of 1/2 swirls, the cosine term merely alternates being -1 or 1, and solutions in the x-position can now be described as [9]

$y>0$ $$x_n = g_1*(-1)^{2N} \quad (2.14)$$

$y<0$ $$x_n = g_2*(-1)^{2N} + \delta \quad (2.15)$$

where g_1 and g_2 are arbitrary constants that depend on the current ray position, N denotes the number of swirls and is restricted to be multiples of 1/2, and $\delta = \frac{B}{1-b} tan(\theta)$, which represents the linear term in (2.13).

We can now iteratively analyze the ray position for every half of a swirl as presented in Table 1. For every half swirl, we first determine which mirror the ray hits and what equation we will apply. Then we need to update the values of g_1 or g_2 according to the current ray position. For instance, when the ray enters the system at $-x_0$, it hits M2+, so equation (2.14) is used. Subsequently, the value of g_1 is determined to be $-x_0$. After a half swirl, the beam hits M2-, and the current beam position in x becomes $+x_0$. When applying equation 2.15 and solve for g_2, we obtain $g_2 = (-x_0 + \delta)$. When we continue this analysis for more swirls, remarkably, we demonstrate that for each swirl, the ray's position is linearly shifted by $\Delta x = 2\delta$. This is significant because we can control the number of swirls (and thereby the time delay) by adjusting the angle of rotation for M2-; the smaller the angle, smaller the Δx, and hence the more the swirls and the longer the time delay. Table 2.1[9] also shows that an addition of 1/2 a swirl negates the position of the ray.

Table 2.1: Iterative Analysis of the Ray Position for Every Half Swirl [9]

N (swirls)	Mirror Hit	Current x-position x_n	Current Equation	g_1	g_2
0	M2+	$-x_0$	(2.14)	$-x_0$	/
1/2	M2-	x_0	(2.15)	/	$-x_0 + \delta$
1	M2+	$-x_0 + 2\delta$	(2.14)	$-x_0 + 2\delta$	/
3/2	M2-	$x_0 - 2\delta$	(2.15)	/	$-x_0 + 3\delta$
2	M2+	$-x_0 + 4\delta$	(2.14)	$-x_0 + 4\delta$	/
5/2	M2-	$x_0 - 4\delta$	(2.15)	/	$-x_0 + 5\delta$
3	M2+	$-x_0 + 6\delta$	(2.14)	$-x_0 + 6\delta$	/

The analysis for the *x*-slope yields similar results. For each full swirl, the Robert cell adds on $\Delta S_x = 2\frac{(1-A)}{(1-b)}\tan(q)$ to the previous slope value. Usually, ΔS_x is a very small quantity on the order of 0.01. Any additional 1/2 swirl flips the sign of the previous slope value.

2.2.4. Robert Cell Properties

The implications of the mathematical solutions can be summarized into the following properties of a Robert cell system with *N* swirls: [9]

Property 1, position in *y*:

For $n = N*K$ cycles, the position in *y* is the same as that of the input, $y_n = y_0$.

Property 2, slope in *y*:

For $n = N*K$ cycles, the slope in *y* is the same as that of the input, $(S_y)_n = (S_y)_0$.

Property 3, position in *x*:

For every swirl, the position in *x* shifts by Δx that is calculated as:

$$\Delta x = 2 * \frac{B}{1-b} tan\,(\theta) \tag{2.16}$$

After *N* swirls, the ray's position in *x* becomes $x_n = x_0 + N*\Delta x$.

Property 4, slope in *x*:

For every swirl, the slope in x shifts by a small quantity ΔS_x calculated as:

$$\Delta Sx = 2 * \frac{(1-A)}{(1-b)} tan(\theta) \tag{2.17}$$

After N swirls, the ray's slope becomes $(S_x)_n = (S_x)_0 + N*\Delta S_x$.

Property 5, additional 1/2 swirl:

For any additional 1/2 swirl, the ray's positions and slopes simply are simply the negative of their previous states.

Of all the properties of the Robert cell, Property 4 is the most unusual and intriguing. Unlike many commonly used optical components, the device adds a constant angle in the x-direction to an input ray regardless of the input angle. This is different from a mirror or a prism, the former of which reflects a beam at the same angle as the angle of incidence, and the latter of which rotates the beam's angle by a quantity determined by the input angle.

2.2.5. Imaging conditions

To practically implement a delay element into a White cell-based system, the delay device should allow the input of a set of beams focused to an array of spots, and the delay element's output beams should also be focused. For a Robert cell system, there are three degrees of freedom with parameters R_1, R_2, and d. These parameters must be chosen to satisfy the periodicity constraint in (2.1) and the input-output focusing constraint. On top of that, one can

specify a distance d to obtain the desired time delay increment. Therefore, we have three variables and three equations to solve.

For the output beam to image, we chose to design Robert cells that focus the beams for every 1/2 swirl, or $K/2$ cycles, in which case the beam will also be focused at the output after N or N+1/2 swirls.

We obtain the equation that satisfies imaging using the ray matrix analysis. For a general ray transfer matrix $\mathbf{H} = \begin{pmatrix} A & B \\ C & D \end{pmatrix}$, if $B = 0$, then the imaging condition is satisfied. Note that the imaging condition for the Robert cell is the same as that of the Herriott cell provided that the angle of rotation θ is small, so we can work with (2.4) to determine the transfer matrix after $K/2$ cycles by extracting the B value of the matrix $\mathbf{T}^{K/2}$.

The B value is a function of R_1, R_2, and d, and it is typically a complicated nonlinear equation. Combined with the periodicity constraint, the values of R_1, R_2, and d are best solved numerically. If we want a cell to have a time delay of 2 ns per swirl with a periodicity of $K = 8$, we can set the distance between the mirrors to be $d = 37.5$ mm. To satisfy both the imaging and the periodicity constraint, the radii of focus are calculated to be $R_1 = 258$ mm and $R_2 = 26.7 \times 10^3$ mm $\approx \infty$. [9]

The mirror parameters above are simulated in ZEMAX. The input to the system is chosen to be a focused circular array of beams. Figure 2.5(a) shows the ray trajectory (side view), and we can see the swirling pattern as expected. Figure 2.5(b) shows the end view, illustrating the spot arrangements each time the beams are focused. The black circle indicates the Airy disk, and it has a radius of 125.8 microns for this Robert cell system. We can see from Figure 2.5(b) that the spots are well within the boundaries of the Airy radius, which means that they are properly focused.

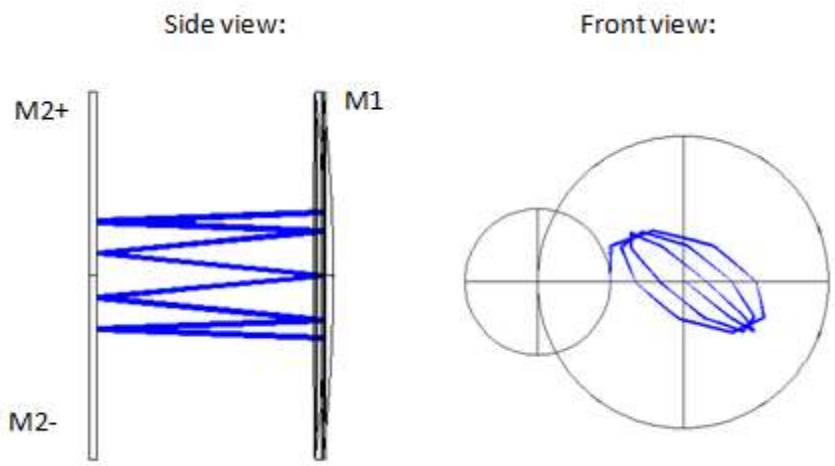

(a)

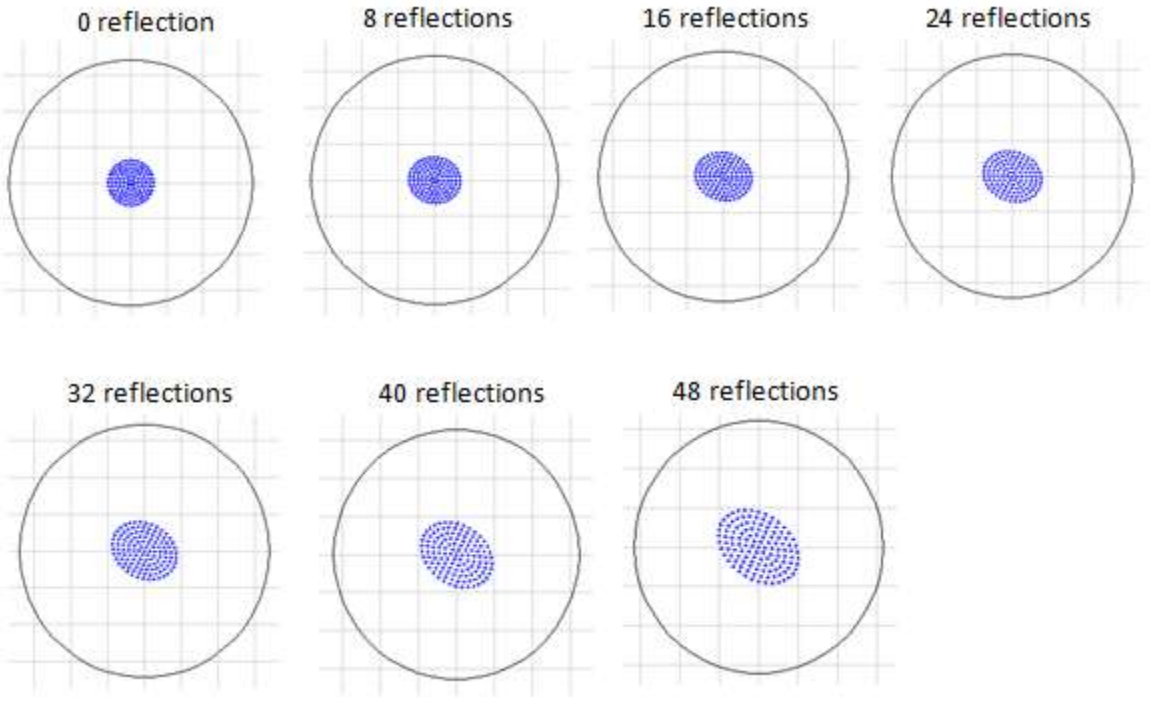

(b)

Figure 2.5: ZEMAX simulation showing that the spots are focused after 49 reflections. (a) The front view and side view of the ray trajectory. (b) The arrangement of spots each time they focus

One potential source for concern would be the accumulation of aberrations over potentially tens and hundreds of bounces. To minimize the aberrations (specifically astigmatism due to beams striking spherical mirrors at varying angles), two solutions present themselves. One option is to keep the angles of incidence small, which means lengthening the cell. While this also reduces the total number of bounces for a given delay, and thus further reduces aberration; it has to be traded off against the larger overall size. Another potential solution is to use toroidal mirrors to correct for astigmatism. The use of astigmatic mirrors in a Herriot cell will perturb the spot pattern [11]; probably the degree of astigmatism needed to correct the aberration due to off-axis beams is small enough not to affect the spot placement significantly, but would have to be accounted for during the design process. In previous work with White cells [3], a path containing 40 mirror reflections had very little loss due to aberration, using a combination of these two approaches (f#>10 and very slightly toroidal mirrors). [9]

2.2.6. The White cell's relation to the Robert cell

As mentioned before, the White cell can be considered as a special case of the Robert cell. In a Herriott cell, when M2 is split in half, it creates a three-mirror system, where M2+ and M2- share the same center of curvature. However, when M2- is rotated by a small angle, its center of curvature (CC) is shifted slightly from that of M2+, which is equivalent to the way mirrors A and B have slightly different CC's [8]. Furthermore, the spot patterns of the Robert cell and the White cell have analogous characteristics. In each cycle, the White cell produces spots that are in rows on mirror C, whereas Fig. 5 shows that the Robert cell creates rows of spots for every $K/2$ cycles. Moreover, the Robert cell's mathematical formalism suggests that if $R_1 = R_2 = d$, rows of

spots can be produced during each cycle without any intermediate spots. Therefore, the White cell is a case of the Robert cell whose radii of curvatures for all of the mirrors are equal to their distance of separation [8].

Chapter 3

Modified Herriott Cell and Robert Cell Devices

While Herriott cells and Robert cells show desirable traits as compact optical TTD devices, we propose that they can be further modified to improve their performances, especially when we couple two Herriott or Robert cells in specific ways. This chapter will be dedicated to discussing three different ways of coupling Herriott cells and Robert cells to produce very long delays to achieve the requirements of an optical TTD system.

3.1. Double Linked-Herriott Cells

3.3.1. Structure and spot patterns

The linked Herriott cell is a novel design that places two Herriott cells right next to each other such that they can share a common flat mirror in the middle as shown in Figure 3.1(a). Cell 1 (also known as the primary cell) and Cell 2 (also known as the secondary cell) have elliptical spot patterns with different periodicities K_1 and K_2, where K_1 and K_2 have a least common multiple of 1. On the common mirror M2, we can place apertures at the locations where the spots in Cell 1 land to allow beam to travel from one cell to the other, and thereby Cell 1 and Cell 2 are linked. When a beam in Cell 1 strikes an aperture on M2, instead of being reflected, it goes into

Cell 2 to experience more reflections before it is returned back to Cell 1. When a beam enters Cell 1 from Cell 2 through an aperture, the Herriott-cell properties of Cell 2 guarantee that the output beam acts as a reflection of the input beam, thus preserving the elliptical spot patterns of Cell 1.

Figure 3.1(b) shows an example of spot patterns of a linked Herriott cell, where in each cell, the periodicities are $K_1 = 5$ and $K_2 = 3$. When a beam enters Cell 1, if M2 does not have any apertures, then the beam would simply form five spots on M1 and M2. Nonetheless, we place two apertures on M2 at the locations of the second spot (rectangle) and third spot (triangle). Thus, when the beam hits the first aperture (rectangle), it travels to Cell 2 and forms a three-spot pattern shown as the rectangular spot patterns. As the beam hits the second aperture (triangle), it once again goes into Cell 2 and forms another three-spot pattern shown as triangles.

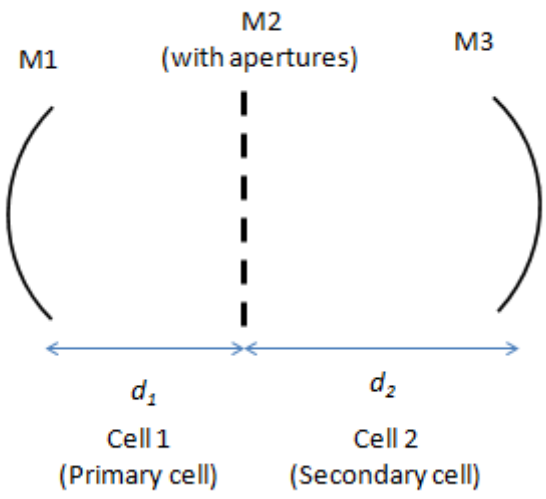

(a)

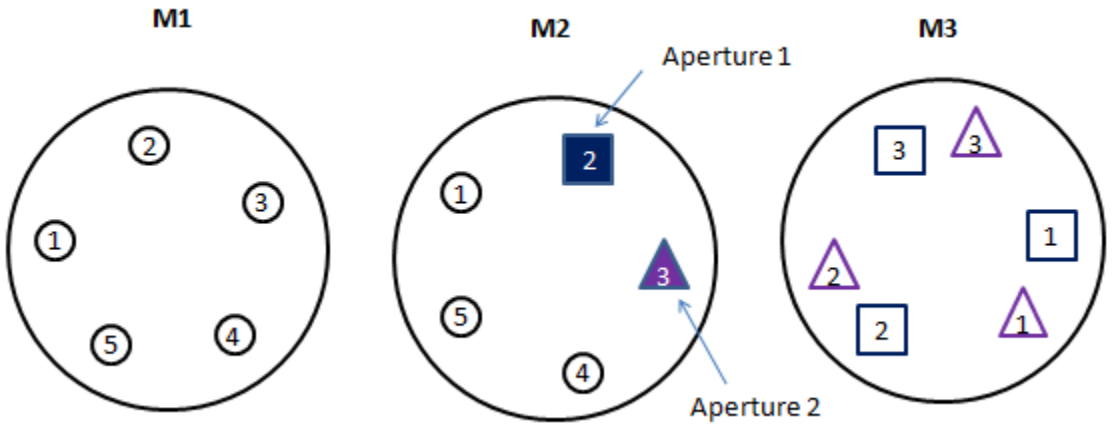

(b)

Figure 3.1: Double linked Herriott cell. (a). The structure. (b). Sample spot pattern

The linked Herriott cell can further be modified to allow multiple locations, each of which corresponds to a different time delay. Figure 3.2 shows an example with two input locations; one is denoted by a circle and the other by a square. The "circle" pattern has two intermediate apertures (the pentagon and the triangle), whereas the "square" pattern has one aperture. As beams enter from each input location into Cell 1, they will trace out unique elliptical spot patterns. We can then specify the number of apertures that is applied to each spot pattern, which determines how many times the beams go from Cell 1 into Cell 2. The amount of time delay at each input location increases with the number of apertures, and different number of apertures can result in different time delays.

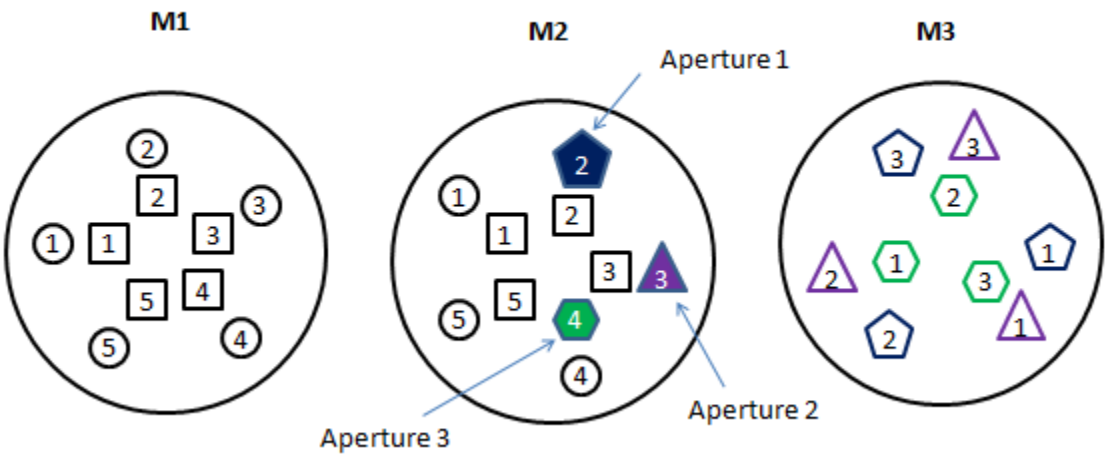

Figure 3.2: The spot pattern of a linked Herriott cell with two input locations. The outer input location has two intermediate apertures, whereas the inner input has one aperture

The linked Herriott cell with multiple inputs and variable time delays is especially useful if it is combined with White cell-based TTD devices, which require their delay elements to have multiple input locations that produce incremental time delays.

3.1.2. Middle mirror design and experiment

As a proof of concept, we aimed to build and test a double linked Herriott cell. We used spherical mirrors M1 and M3 both with radii of curvatures of 100mm, and we designed a middle mirror with four sets of apertures on a big piece of glass. This was intended for us to go through only one manufacturing process and still obtain multiple sets of apertures for our experiment. The middle mirror, shown in Figure 3.3, was manufactured using a metal masking technique from Gentex Corporation. Initially, we had intended to design four sets of outer and inner

patterns, whose outer aperture to inner aperture ratios are 1:0, 2:1, 3:2, and 1:2. However, the manufacturer misinterpreted our drawing, and they produced middle mirror with outer to inner aperture ratios of 1:0 (top left), 6:6 (top right), 3:2 (bottom left), and 4:4 (bottom right). Unfortunately, the apertures with ratios of 6:6 and 4:4 do not produce different delays.

Figure 3.3: Aperture design manufactured by Gentex Corporation

As of now, a spot pattern has been created with the simplest design, where the outer/inner aperture ratio is 1:0. The spot pattern of the linked Herriott cell is shown in Figure 3.4, which shows spots formed in both the primary cell and the secondary cell. The periodicities in cell 1

and cell 2 are: K_1 = 4, and K_2 = 5. Evidently, the beam passed through the aperture to form an elliptical pattern on the secondary cell, and then it returned to the primary cell to complete its cycle of operation.

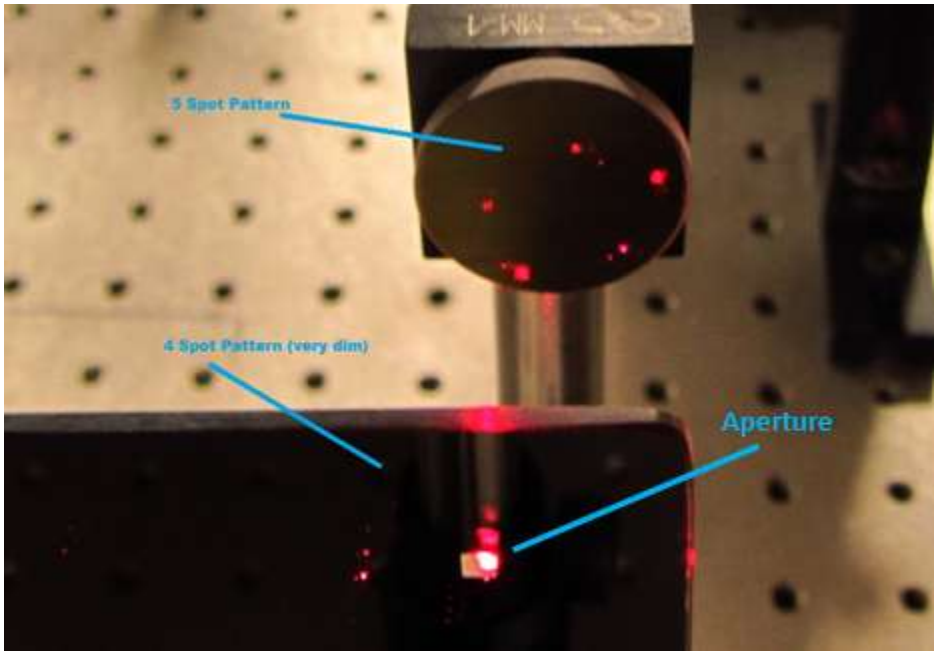

Figure 3.4: Spot pattern formed with a double linked Herriott cell with one aperture

3.2. Coupled Robert Cell for Binary White Cell-based True-time Delay

In Section 2.2.4, we described the properties of the Robert cell in N and N+1/2 swirls. With these properties, we designed various modifications to improve the performance of the Robert cell as an optical delay device. We first made adjustments to the mirror shapes of a single cell as to accept beams from various input locations. We then created two different ways of coupling the adjusted Robert cells to create longer delays.

3.2.1. Variable time delays within a single cell

The first set of modifications to the Robert cell is that M2+ and M2- can be shaped such that the device allows the rays to enter and exit from different positions whose *x*-coordinates are multiples of $\Delta x/2$. Each input location also corresponds to a different amount of delay. The schematics of these two designs are displayed in Figure 3.5 [9], which shows three different input locations that are labeled with different colors. In Figure 3.5(a), mirror M2 is shaped for beams to enter from one side and exit out of the other; in Figure 3.5(b), M2 is shaped for beams to enter and exit from the same side. All intermediate spots are hidden except for those that have undergone multiples of $K/2$ cycles (or half a swirl), and they are indexed in terms of K with their corresponding colors. Part (a) shows a design that allows the beam to make a full N swirls, whereas the design in part (b) allows the beam to make $N+1/2$ swirls. By cutting off the edges of mirrors M2+ and/or M2-, only the input and output locations miss the mirrors to communicate with the space outside and all intermediate reflections are contained within the cell. For input locations farther from the center of the device, the ray experiences more swirls and thus carries a longer time delay.[9]

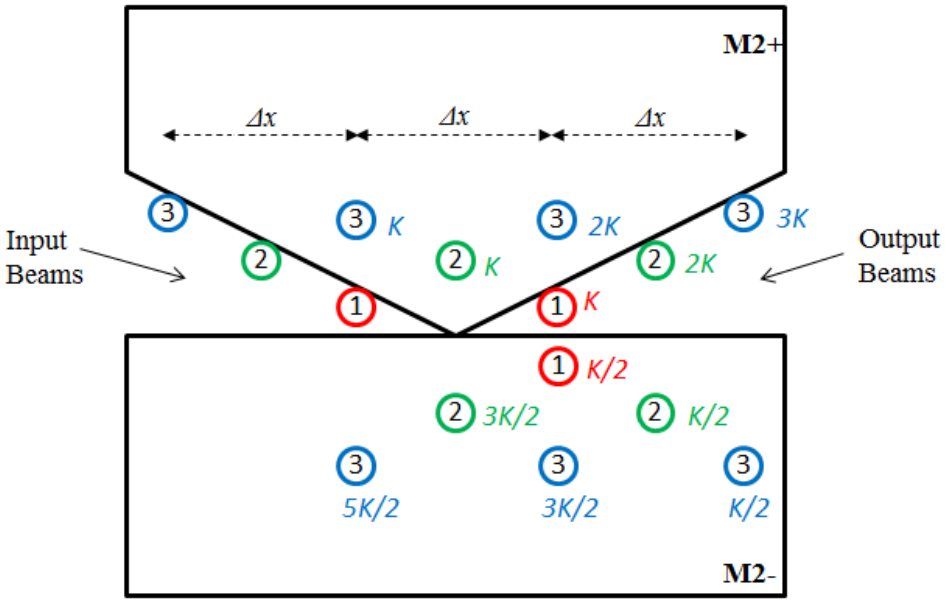

(a)

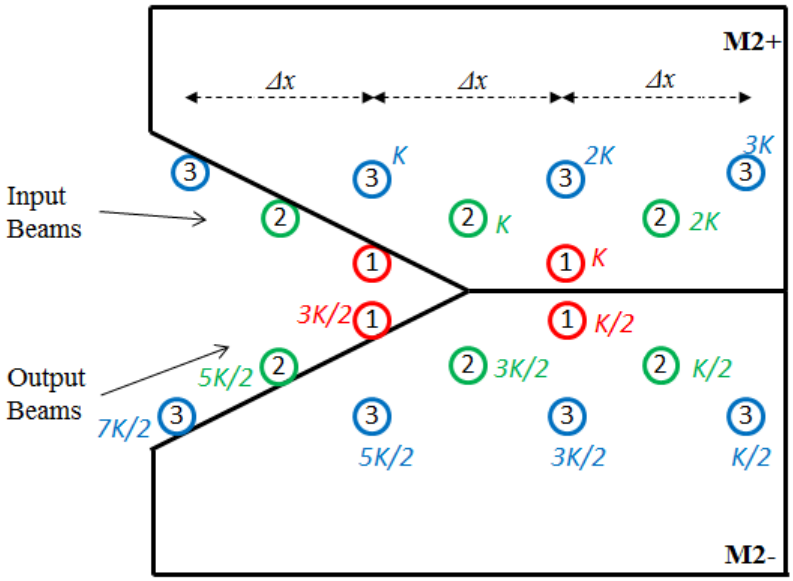

(b)

Figure 3.5: The front view of the Robert cell designs that allow beams to enter from different input locations to achieve different time delays. Part (a) allows beams to exit after full N swirls, whereas part (b) allows beams to exit after N+1/2 swirls. [9]

The input and output conditions are different for these two schematics. For the device shown in Figure 3.5(a), the Cartesian coordinate of their input and output relationships are [9]:

$$x_{out} = -x_{in}$$

$$y_{out} = y_{in}$$

$$(S_x)_{out} = (S_x)_{in} + \gamma_1$$

$$(S_y)_{out} = (S_y)_{in} \tag{3.1}$$

Equation (3.1) can also be represented pictorially as shown in Figure 3.6(a). For a Robert cell that performs N swirls, the input beam position is reflected about the y-axis. The output beam slopes relate to the input slopes as follows: In the y direction (see side view), the slope of return equals to that of incidence, just as a mirror; in the x direction (top view), the slope is also similar to a beam striking a mirror, except the slope in the x-direction is additionally rotated by a small quantity γ_1, which is specified by the angle offset due to the tilt of M2-.

Whereas, for the device in Figure 3.5(b) [9],

$$x_{out} = x_{in}$$

$$y_{out} = -y_{in}$$

$$(S_x)_{out} = -(S_x)_{in} + \gamma_2$$

$$(S_y)_{out} = -(S_y)_{in}. \tag{3.2}$$

The relationships in equation (3.2) are also depicted in Figure 3.6(b) [9], which shows that for a Robert cell that performs N+1/2 swirls, the input position is reflected across the x-axis. The

output beam travels in a direction that is almost anti-parallel to the input beam, except that the slope in the *x*-direction is rotated by γ_2.

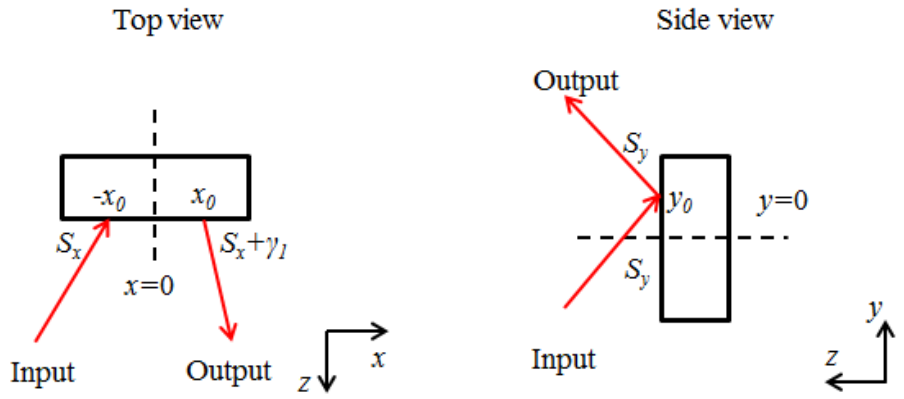

(a)

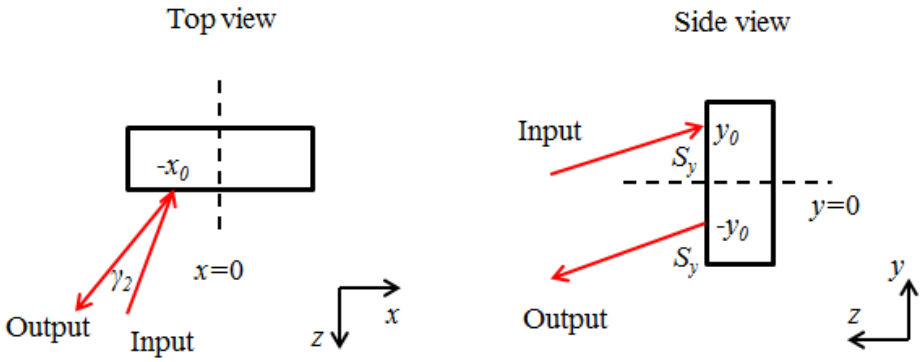

(b)

Figure 3.6: The top and side view illustrations of the Robert cell input and output relationships. (a) shows a device that performs full *N* swirls, and (b) shows a device that performs *N+1/2* swirls. [9]

3.2.2. Coupled Robert cell as a delay element for the binary White cell

As discussed in section II, the binary White cell needs a delay plane whose amount of delay varies with the input position. Thus, both of the Robert cell configurations in Figure 3.5 are compatible to this requirement. We choose to adopt the design in Figure 3.5(a) because all of its swirls are full integers, making its analysis easier. Because the input positions of the Robert cell are slanted, the cell needs to be rotated such that a line joining the input locations is vertical as shown in Figure 3.7 [9], so that it matches the arrangement of the light beams on the MEMS.

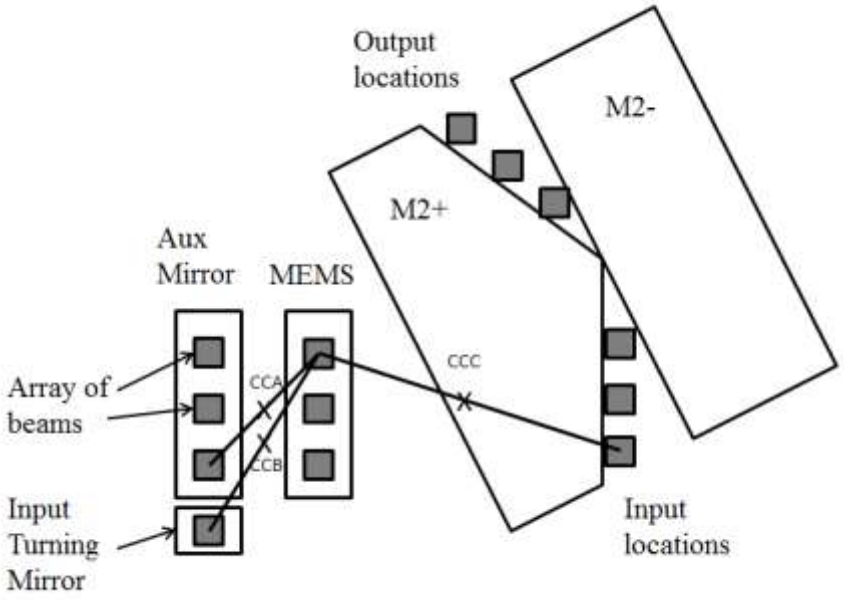

Figure 3.7: Employing a single modified Robert cell as a delay plane for the Binary cell. Unfortunately, a line connecting the output locations is not parallel to a line connecting the input locations. [9]

Now, however, the line joining the output beam locations is not parallel to the line of input beam locations. Normally in the White cell, the beams leaving the delay plane are re-imaged onto the MEMS by a single objective mirror, e.g. Mirror D in Figure 1.7. The input beams to the Robert

cell are in a vertical column, but the output beams from the Robert cell are on a diagonal, which will not map to the MEMS columns properly. If we would like to keep this design, we will have to use one spherical mirror for each output position to re-image the beams onto the desired MEMS locations.

The addition of many spherical mirrors can make the system somewhat cumbersome. A better solution is coupling two Robert cells using the integer-swirl design in Figure 3.5(a) (as opposed to coupling two half-integer-swirl designs as in Figure 3.5(b)), using a spherical mirror E. The new design's top-view schematic is shown in Figure 3.8(a), and its front view with Mirror E's center of curvature is shown in Figure 3.8(b). When an array of input beams is sent into an input location of Cell 1, mirror E images the output beams of Cell 1 onto the corresponding input location of Cell 2. Figure 3.8(b) demonstrates that the line connecting the output locations of the second cell is parallel to the line connecting the input locations. This makes it possible to use spherical mirror D to send the beams to the auxiliary mirror and then back onto the next column of the MEMS. Figure 3.8(c) provides one example of the spot patterns formed in the case where the beams are switched into the delay plane by the MEMS. The indices 0 through 7 show the order of the spot locations. At the end of step 7, the output beams from the coupled Robert cell system are imaged onto the next column of the MEMS as desired. [9]

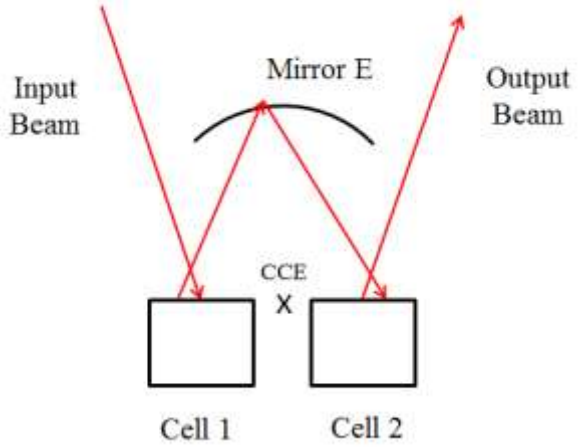
Input
Beam
Mirror E
Output
Beam
CCE
Cell 1
Cell 2

(a)

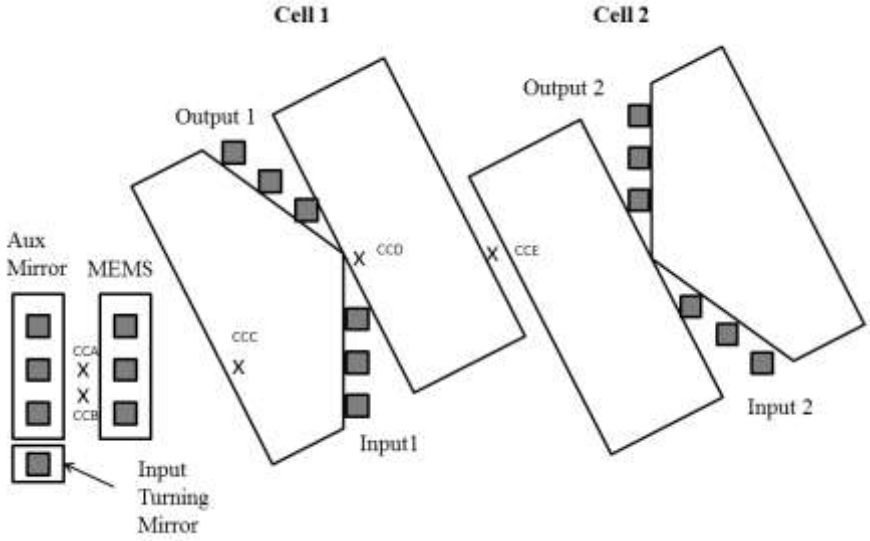
Cell 1
Cell 2
Output 1
Output 2
Aux
Mirror
MEMS
CCA
CCB
CCC
CCD
CCE
Input1
Input 2
Input
Turning
Mirror

(b)

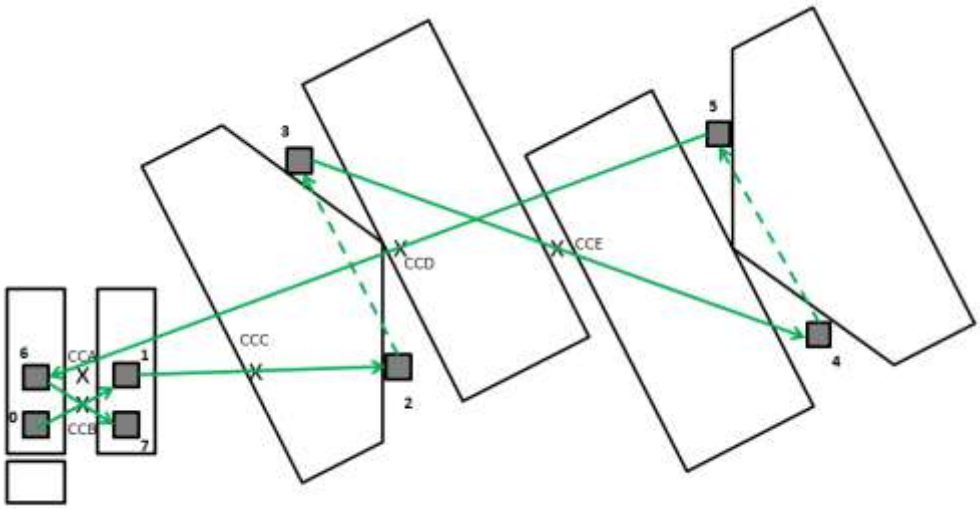

(c)

Figure 3.8: Combining a duel Robert cell with a TTD system. (a) Top view of the dual Robert cell system coupled with mirror E used as a delay plane. (b) The structure of the coupled Robert cell showing all the possible beam spots. (c) The trajectory of a beam if it [9]

When the Robert cells are integrated into the White cell, they are placed at the delay plane location as seen in Figure 3.9 [9]. As a set of beams is selected to be delayed, the MEMS can reflect the beams onto mirror C, which sends the beams into the first Robert cell. The beams eventually come out of the second Robert cell, whereupon they diverge onto mirror D, which focuses the beams back onto the next row or column of the MEMS.

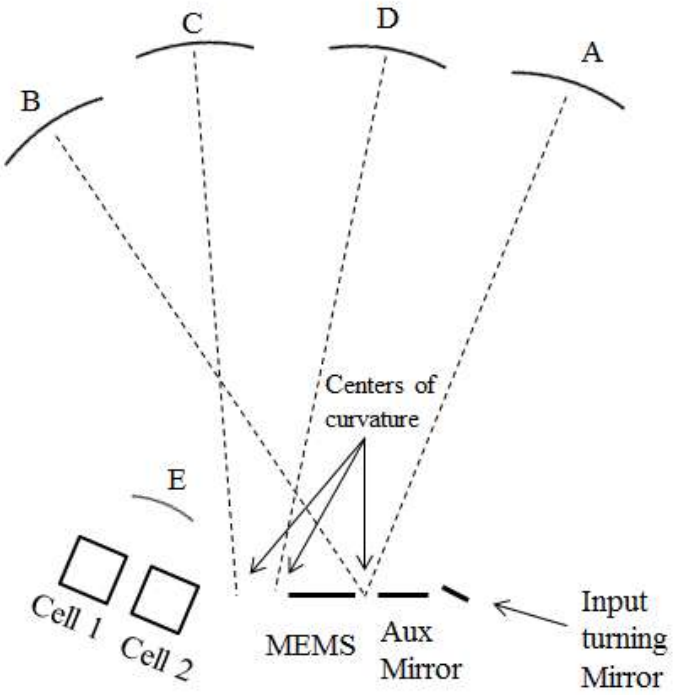

Figure 3.9: Top view of a White cell-based TTD device that uses the Robert cell as its delay plane. [9]

During the *n*-th cycle of the binary White cell, while a traditional delay plane produces a delay that is proportional to 2^n, the Robert cell provides a delay proportional to *n*. Thus, over *n* cycles of operations with the smallest time increment Δ, the maximum achievable time delay for the Robert cell, $[n(n+1)/2]\,\Delta$, much similar to a quadratic White cell [10].

3.3. Coupled Robert Cell for ultra-long time delay

To create much longer time delays, two Robert cells can be coupled using a spherical mirror. For ultra-long delays, two of the same cells shown in Figure 3.5(b) are used as shown in Figure 3.10. This looks similar to the device in Figure 3.9, except that instead of the beam coming from the White cell, and visiting each Robert cell *N* swirls one time each before returning to the White cell, now the beam volleys back and forth between the two Robert cells multiple times before exiting. When a beam first enters cell 1, it exits after *N*+1/2 swirls and impinges onto the auxiliary spherical mirror M_A. Mirror M_A's center of curvature is positioned such that it reflects the output of the first Robert cell onto the input of cell 2, whose output returns back into the input of cell 1 via M_A at the new location. The beam is delayed further, and returns to the second Robert cell again at a new location. Thus, the input beam bounces back and forth between these two cells some number of times, accumulating very long delays. Due to the small angular rotation γ_2 in (22), the ray is slowly rotated to the left for every time it enters a cell, and the beam will eventually miss mirror M_A and exit from the output position of cell 2.[9]

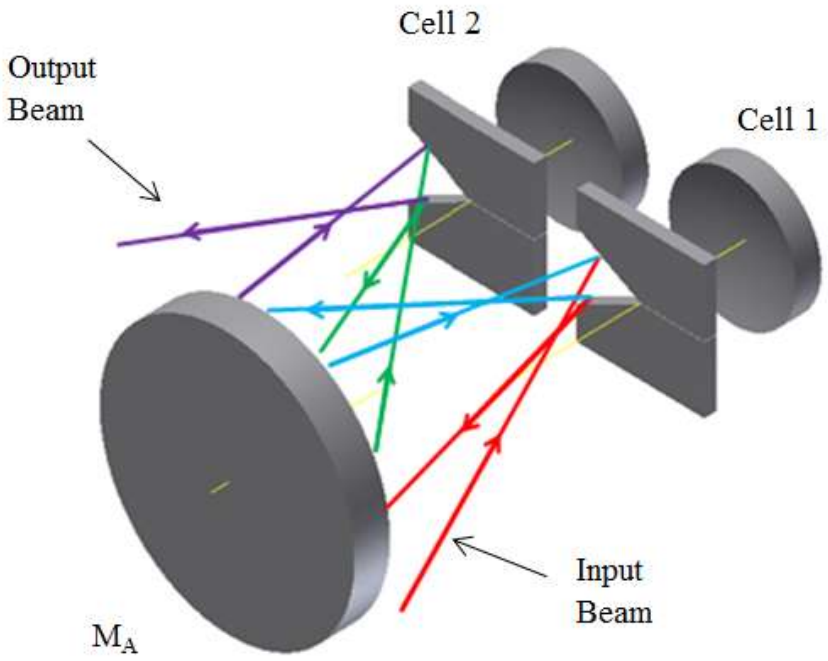

Figure 3.10: Coupled Robert cell system. Mirror MA is placed such that the output of one cell is reflected to the input of the other cell. [9]

A single Robert cell that has a mirror separation of a few centimeters can achieve a delay on the order of 10 ns. With the coupled Robert cell, however, delays on the order of 100 ns can be easily obtained.

Chapter 4

Summaries

In this document, we have discussed the way by which modified Herriott cells and Robert cells can be used as delay elements for existing optical TTD systems. We first reviewed the components and operations of White-cell based optical TTD systems, and we discussed the requirements for their delay elements. Next, we analyzed the structures of the Herriott cell and the Robert cell, both of which are multipass systems that allow beams to propagate a long distance. Through ray matrix and difference equation analyses, we have derived the spot patterns and the properties of the Herriott cell and the Robert cell, allowing us to design variations as the delay element for the White cell-based TTD system with the Binary cell structure. Compared to traditional delay elements such as glass blocks, lens trains, and optical fibers, the modified Herriott cell and Robert cell systems are not only compact, but they can also achieve long time delays with low loss. Furthermore, ultra-long delays on the order of 100 ns can be attained using a coupled Robert cell design.

References

[1] B. L. Anderson, S. A. Collins, Jr., C. A. Klein, E. A. Beecher, S. B. Brown, "Photonically Produced True-Time Delays for Phased Antenna Arrays," *Applied Optics*, **36**(32), pp. 8493-8503, 1997.

[2] B.L. Anderson, J.G. Ho, W.D. Cowan, O. Blum-Spahn, A. Y. Yi, D.J. Rowe, M.R. Flannery D.L. McCray, P. Chen, and D.J. Rabb, "Hardware Demonstration of Extremely Compact Optical True Time Delay Device for Wideband Electronically Steered Antennas."*Journal of Lightwave Technology*, **29**(9), pp. 1343-1353, May 1, 2011

[3] J. White, "Long optical paths of large aperture," *J. Opt. Soc. Ame.* Vol. 32, No. 2, pp. 285-288, May 1942

[4] R. L. Higgins, N. K. Nahar, B. L. Anderson, "Design and demonstration of a switching engine for a binary true-time-delay device that uses a White cell," *Applied Optics*, **42**(23), pp. 4747-4757, 2003.

[5] B. L. Anderson, D. J. Rabb, C. M. Warnky, F. M. Abou-Galala, "Binary Optical True Time Delay Based on the White Cell: Design and Demonstration,"*IEEE Journal of Lightwave Technology*, ," *IEEE Journal of Lightwave Technology*, **24**(4), pp. 1886-1895, April, 2006.

[6] S. Kunathikom, B. L. Anderson, S. A. Collins, Jr., "Design of delay elements in binary optical true-time delay devices," *Applied Optics*, **42** (35) pp. 6984-6994, December 2003.

[7] Christopher G. Tarsitano and Christopher R. Webster, "Multilaser Herriott cell for planetary tunable laser spectrometers," Appl. Opt. **46**, 6923-6935 (2007).

[8] Claude Robert, "Simple, stable, and compact multiple-reflection optical cell for very long optical paths," *Applied Optics*, **46** (22) pp. 5408-5418, August 2007

[9] Y.Shi, B.L. Anderson, "Robert cell-based optical delay elements for White cell True-time delay devices,"*Journal of Lightwave Technology*, **31**(7), pp. 1006-1014, April 1, 2013

[10] B. L. Anderson, C. D. Liddle, "Optical true-time delay for phased array antennas: demonstration of a quadratic White cell," *Applied Optics*, **41**(23), pp. 4912-4921, 2002.